Check for updates

JGR Solid Earth

RESEARCH ARTICLE
10.1029/2025JB032783

Increasing the Accuracy and Efficiency of Micromagnetic Tomography by Double Sided Scanning

Frenk Out[1], Rosa A. de Boer[1], Martha E. Kosters[1], Bertwin M. de Groot[1], and Lennart V. de Groot[1]

[1]Paleomagnetic Laboratory Fort Hoofddijk, Department of Earth Sciences, Utrecht University, Utrecht, The Netherlands

Key Points:

- Both the accuracy and the efficiency of Micromagnetic Tomography experiments are improved by making magnetic scans on both sides of a sample
- Double-sided scanning doubles the amount of numerically stable magnetic moments obtained from a sample compared to one-sided scanning
- After applying a numerical proxy we retain a quarter of the magnetic moments of all carriers for double-sided scanning in natural samples

Supporting Information:

Supporting Information may be found in the online version of this article.

Correspondence to:

R. A. de Boer,
r.a.deboer1@uu.nl

Citation:

Out, F., de Boer, R. A., Kosters, M. E., de Groot, B. M., & de Groot, L. V. (2026). Increasing the accuracy and efficiency of micromagnetic tomography by double sided scanning. *Journal of Geophysical Research: Solid Earth*, *131*, e2025JB032783. https://doi.org/10.1029/2025JB032783

Received 19 AUG 2025
Accepted 10 DEC 2025

Author Contributions:

Conceptualization: Frenk Out, Martha E. Kosters
Data curation: Frenk Out
Formal analysis: Frenk Out
Funding acquisition: Lennart V. de Groot
Investigation: Frenk Out, Rosa A. de Boer, Martha E. Kosters, Lennart V. de Groot
Methodology: Frenk Out, Rosa A. de Boer, Martha E. Kosters, Bertwin M. de Groot
Project administration: Lennart V. de Groot
Resources: Rosa A. de Boer, Bertwin M. de Groot

© 2026. The Author(s).
This is an open access article under the terms of the Creative Commons Attribution License, which permits use, distribution and reproduction in any medium, provided the original work is properly cited.

Abstract Paleomagnetic data are usually retrieved by subjecting bulk samples, for example lavas, to laboratory measurement protocols. In many instances, the data related to these protocols yield uninterpretable results caused by the presence of particles with adverse magnetic properties that blur the signal of the reliable magnetic particles. With Micromagnetic Tomography (MMT) we focus on identifying the signal of particles with reliable properties. Their individual magnetic moments are computed by scanning the surface of a ~3 mm^2 thin section with a quantum diamond microscope (QDM) and locating the magnetic recorders with computed tomography. Currently, the largest portion of all resolved magnetic moments is discarded due to numerical instability, making it difficult to obtain statistically relevant paleointensities and paleodirections based on the remaining magnetic moments. We improve the number of reliable magnetic moments from MMT experiments by making a QDM scan of both sides of the sample. Here, we conduct a combined numerical and empirical study to investigate the benefits and difficulties of adding this double-sided scanning (DSS) protocol to MMT. By investigating the theoretical gain of DSS for varying sample thicknesses, we show that DSS returns twice more numerically stable magnetic moments compared to single sided scanning for a sample thickness of 60 μm. By overcoming practical difficulties related to sample preparation and scanning, DSS will provide a significant boost in retrieved stable magnetic moments.

Plain Language Summary Magnetic grains in volcanic rocks may obtain a magnetic signal when cooling in the presence of Earth's magnetic field. However, only a fraction of all grains record the signal well. To find these stable grains, we apply a new paleomagnetic technique called Micromagnetic Tomography (MMT): a tool that computes the magnetic signal of individual grains. For this purpose, a thin rock slice is scanned for the magnetic signal near the sample surface and the location of magnetic recorders in the sample. These data sets are combined to determine the magnetic signal per grain. However, most grains resolved with MMT are currently disregarded, because their results are very susceptible to measurement noise; the remaining recorders are not sufficient to obtain a reliable reconstruction of Earth's magnetic field. That is why we improve the number of reliable magnetic moments by scanning not only the top, but also the bottom of a rock sample. Adding this information doubles the number of numerically stable recorders compared to a one-sided magnetic scan. With this increased number of retrieved recorders, we can better estimate statistically relevant paleomagnetic information.

1. Introduction

The past state of Earth's magnetic field is recorded by volcanic and sedimentary rocks when they are formed. By taking samples of such rocks and measuring their magnetic moment, the paleomagnetic information stored in them can be deciphered. Paleomagnetic information is usually described by a paleodirection and a paleointensity. These are retrieved by subjecting bulk samples to laboratory treatments, such as thermal or alternating field demagnetization and paleointensity protocols. Depending on the type of the sample, paleodirections are relatively easy to extract, but only a small part (10%–20%) of the paleointensity experiments produce a result that passes sufficient selection criteria (Tauxe & Yamazaki, 2015). This low success-rate is mainly caused by the difference in how individual magnetic recorders in a paleomagnetic bulk sample store the ambient magnetic field. Depending on particle size, particle shape, chemical composition, and other external factors, these recorders acquire a signal that aligns, partially aligns, or does not align with the imposed magnetic field (e.g., Dunlop & Özdemir, 1997; de Groot et al., 2021; Nagy et al., 2017). If the magnetic signal of these poorly aligned recorders overshadow the signal of good recorders, retrieving a reliable paleointensity from bulk sample is difficult.

21699356, 2026, 1, Downloaded from https://agupubs.onlinelibrary.wiley.com/doi/10.1029/2025JB032783, Wiley Online Library on [07/11/2026]. See the Terms and Conditions (https://onlinelibrary.wiley.com/terms-and-conditions) on Wiley Online Library for rules of use; OA articles are governed by the applicable Creative Commons License

Software: Frenk Out
Validation: Frenk Out
Visualization: Frenk Out
Writing – original draft: Frenk Out, Rosa A. de Boer
Writing – review & editing: Frenk Out, Rosa A. de Boer, Martha E. Kosters, Bertwin M. de Groot, Lennart V. de Groot

By selecting the individual magnetic contributions of the most reliable particles we might improve the success rates for obtaining paleointensities. The magnetic moment of these individual magnetic particles can be obtained from Micromagnetic Tomography (MMT), a new technique that combines information on the position of these magnetic carriers and their magnetic signal (de Groot et al., 2018). The position of magnetic carriers, usually iron-oxides, is determined by nano X-Ray computed tomography (NanoCT); in NanoCT images these magnetic carriers (>500 nm) show up as bright, high-density, spots amidst other low-density minerals. The magnetic field produced by these carriers is measured with a quantum diamond microscope (QDM). QDM has a very high resolution (∼1 μm), and a field of view of ∼3 mm^2 (e.g., Glenn et al., 2017; de Groot et al., 2021; Kosters et al., 2023). Hence, the samples studied by MMT are ideally tiny cores with a diameter of ∼1.5 mm.

Magnetic moments have already been successfully retrieved from volcanic samples with MMT (de Groot et al., 2018; Kosters et al., 2023), and the obtained values are in line with expected trends of particle size versus magnetization (Dunlop & Özdemir, 1997). For iron-oxide particles ≤1 μm this trend is not verified since these carriers cannot be imaged by NanoCT yet. However, ongoing development of CT technology will eventually allow a new view on these submicron recorders (Nagy et al., 2017; Out, de Boer, Walmsley, & de Groot, 2024; Out, de Boer, Kosters, et al., 2024). The biggest challenge for MMT lies with the amount of magnetic moments it can accurately solve: depending on the applied cut-off, only a small fraction of the magnetic moments retrieved in MMT studies of de Groot et al. (2018) and Kosters et al. (2023) is numerically stable (Out et al., 2022). These grains return poor results when inverted due to numerical instability. At the current state, grains located deep (>15 μm) in a sample are numerically too unstable to resolve and are not included in subsequent interpretation steps. Missing out on these potentially useful recorders makes it difficult to acquire enough grains for a statistically relevant paleodirection and paleointensity from a single sample (Berndt et al., 2016). Recent findings of Bellon et al. (2025), however, show that the amount of PSD carriers might actually be in the realm of what MMT can achieve. Nevertheless, more magnetic carriers will invoke a more realistic paleomagnetic estimate, hence it is pivotal to increase its output of numerically stable grains per sample for MMT.

Here we show how to increase both the amount and accuracy of numerically stable magnetic moments from MMT by making QDM scans of both sides of a sample, and including them both in the inversion. By using magnetic information on both sides, the magnetic moments of previously deeper grains are now constrained by measurements at the top and bottom of the sample. This confines the range of possible solutions to more realistic values, as previously shown by Reis et al. (2016), who applied this principal to magnetometry data. For regular single-sided scanning (SSS), thick sections (samples >30 μm) are not considered because the uncertainties of the magnetic moments become too high; solving even less numerically stable grains than with thin sections (Out et al., 2022). For SSS this means that almost all retrieved magnetic moments in thick sections have unrealistically high uncertainties. Fortunately, double-sided scanning (DSS) provides a two-sided constraint that should produce more numerically stable resolved magnetic moments in thick sections. Therefore, we investigate the use of thicker samples for DSS as well. On the other hand, DSS might come with some complications: sample handling is more complicated than for SSS, since a rock sample needs to be flipped without breaking to allow two sided QDM measurements. Furthermore, the amount of data is doubled, requiring more efficient algorithms to solve the least-squares inversion problem for all particles (Fabian & De Groot, 2019).

To investigate these costs and benefits of DSS we studied both a numerical and a physical sample. The numerical sample allows controlling sample size, number of grains, individual grain position, and magnetic moment to simulate the properties of the physical samples as close as possible. This numerical sample provides an estimate for the physical sample on how many grains are numerically stable for DSS compared to SSS. The physical sample, on the other hand, will provide valuable insight into the experimental difficulties in preparing a sample for DSS. This combined study of numerical and physical samples will assess whether DSS is an upgrade to the MMT protocol; solving more magnetic moments which leads to statistically relevant paleomagnetic direction and intensity.

2. Numerical Simulations

Computational models establish the framework for acquiring numerically stable magnetic moments in physical samples. The numerical models are created in a similar way to the models described in Out et al. (2022). We modified the algorithm of Cortés-Ortuño et al. (2024) to allow for DSS magnetic moment calculations (cf. *multi_data* branch on github, or see Out, de Boer, Walmsley, and de Groot (2024) and Out, de Boer, Kosters, et al. (2024).

21699356, 2026, 1, Downloaded from https://agupubs.onlinelibrary.wiley.com/doi/10.1029/2025JB032783, Wiley Online Library on [07/11/2026]. See the Terms and Conditions (https://onlinelibrary.wiley.com/terms-and-conditions) on Wiley Online Library for rules of use; OA articles are governed by the applicable Creative Commons License

2.1. Methods

For the numerical study, we created eight numerical rock slices with a surface area of 500 × 500 μm and eight distinct thicknesses (30, 40, 50, 60, 70, 80, 90, and 100 μm) using the *MagneticSample*-class (Cortés-Ortuño et al., 2024). For each rock slice we created 20 different models, summing up to 160 models in total. Each rock slice was populated at random with spherical magnetic carriers with varying grain diameters up to 10 μm, following the grain-size distribution of Out, de Boer, Walmsley, and de Groot (2024) and Out, de Boer, Kosters, et al. (2024). The spatial grain density of the physical sample, described later, is used to set the number of magnetic carriers with a size between 1 and 10 μm: this sample consists of 2,316 particles in a 1.1 × 1.1 mm^2 subsection with a thickness of ∼60 μm which translates to a density of about 30.000 grains per mm^3. Given that this fraction accounts for 0.08% of all magnetic carriers according to Out, de Boer, Walmsley, and de Groot (2024) and Out, de Boer, Kosters, et al. (2024), the number of grains smaller than 1 micron scales to almost 40 million particles per mm^3. We allocated magnetic moment intensities to each carrier according to the grain-size–TRM (thermo-remanent magnetization) trend of Dunlop and Özdemir (1997). The directions of the magnetic moments were randomly assigned, creating a unique dipolar magnetic moment for each grain. After each rock slice was created, we used the allocated magnetic moments to build QDM scans at both sides with a stand-off distance of 2 μm with respect to the top and bottom of the sample. Gaussian noise with a standard deviation of 20 nT was added to all scans (Glenn et al., 2017). Figure 1 shows an overview of modeled magnetic fields for a top and bottom scan.

We realize that assigning magnetic moment in this way is an oversimplification of reality. Given the complex magnetic structures expected in particles larger than one micron, multivortex (MV) configurations are likely present. These can cause a natural stray field to remain strongly non-dipolar over longer distances. In our approach we ignore this effect and treat all particles as solely dipolar magnetic carriers, because we focus in this study on retrieving dipolar components of particles.

In the next step, the magnetic scans were inverted using the position of magnetic carriers larger than 1 micron to reconstruct their respective magnetic moments. With this scenario we modeled the inability of current CT techniques to resolve particles smaller than 1 μm. For SSS we only used the top magnetic scan in the inversion; for DSS both sides were used (see Figure 1). Both SSS and DSS were inverted for magnetic moments using dipole expansions. To assess the error of the inversion, computed magnetic moments ($\hat{m}$) were compared to the true magnetic moments (m). We state that a magnetic moment is well resolved when: $\frac{|\hat{m}-m|}{|m|} \leq 0.1$, with $||$ the euclidean norm. With the signal strength ratio (SSR) we determine which grains are resolved numerically stable. SSR is a proxy based on volume and distance of a grain to the closest sensor (see Figure 1), that assesses which magnetic moments are likely to be numerically well solved (Cortés-Ortuño et al., 2021; Out et al., 2022). Particles with a high SSR are more likely to have a stable magnetic moment than particles with a low SSR. The SSR ($\frac{Vd_0}{r^3 d}$, $d_0 = 10^{-6}$m) is determined by dividing the volume V of the carrier by its diameter d and cubed distance r to the magnetic sensor. This number is multiplied by a grain diameter of d_0: = 1 μm to make the SSR parameter dimensionless. The SSR allows us to separate the numerically stable solutions from the unstable solution in a real sample as well. The cut-off SSR value is determined in the numerical models by plotting SSR per grain against error. We define the cut-off value as the smallest value for which 90% of the grains that pass the SSR, have an error in magnetic moment of 10% or less. Particles with a SSR lower than the cut-off value are hence ignored for their numerical instability. The cut-off value is averaged over the 20 models and determined for each rock slice thickness.

2.2. Results

In Figure 2a the percentage of correctly resolved grains as function of sample thickness is plotted for SSS and DSS scanning for the numerical samples. The relative error is defined as the euclidean norm between calculated and true magnetic moment divided by the norm of the calculated magnetic moment. For SSS, the percentage of well resolved magnetic moments decreases from 15% to 20% for 30 micron thick samples to values below 5% for a sample thickness of 70 micron and larger. The percentage of correctly resolved magnetic moments for DSS is generally twice as high compared to SSS: it decreases from a maximum of 30% to slightly below 10% for 100 micron sample thickness.

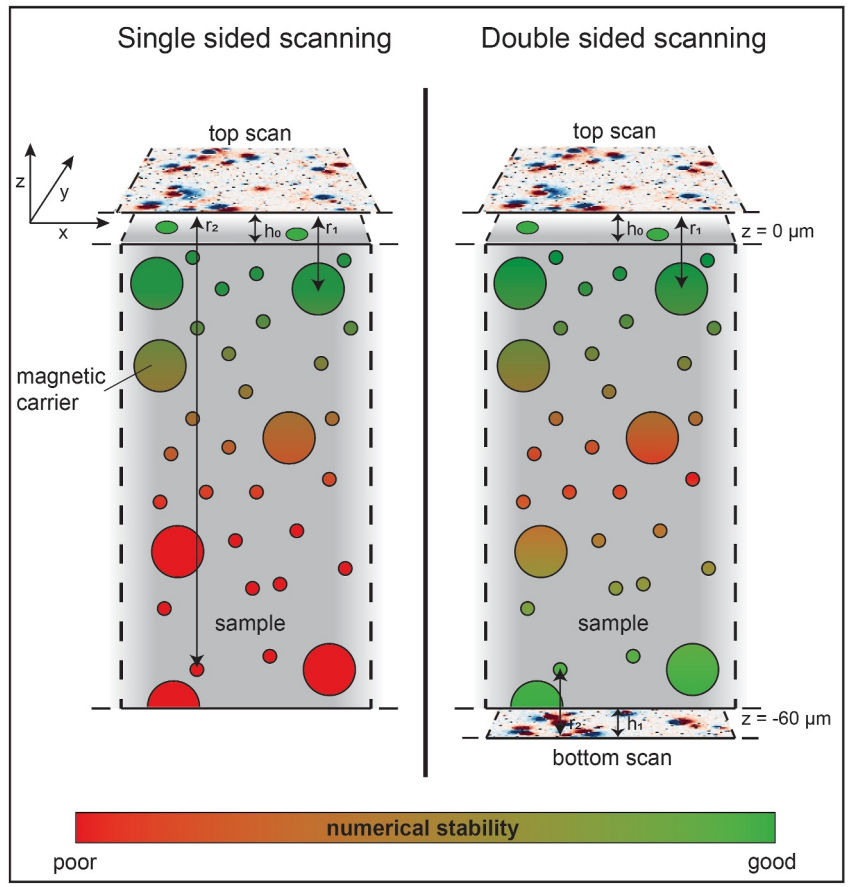


Figure 1. Overview of Double-Sided Scanning (DSS) and Single-Sided Scanning (SSS). In both cases the top of the sample is set to $z = 0$. The top QDM scan is at a distance h_0 from the top of the sample; the bottom QDM scan is located h_1 below the sample. The SSR for DSS is calculated based on the closest sensor plane, where the SSR for SSS is based on the top sensor plane only (see r_1 and r_2). The color of each magnetic carrier is descriptive for whether the solved magnetic moment is expected to be numerically stable (green) or not (red).

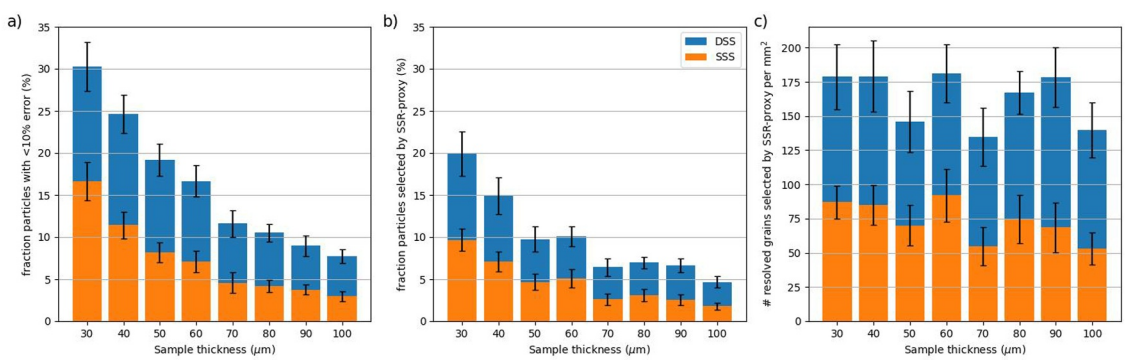


Figure 2. Overview of resolved grains for the numerical samples. (a) Percentage of resolved magnetic moments with an error smaller than 10% (see main text). (b) Percentage of correctly resolved magnetic moments based on the SSR-proxy of 10^{-2}. (c) Number of correctly resolved grains based on SSR-proxy per mm^2 sample surface. The SSR-proxy ensures that 90% of grains have an error <10% (see main text). The single-sided (SSS) results (in orange) are outperformed by double-sided (DSS) scanning (in blue) in all cases. Standard deviations over 20 models per sample thickness are plotted in black for all panels.

21699356, 2026, 1, Downloaded from https://agupubs.onlinelibrary.wiley.com/doi/10.1029/2025JB032783, Wiley Online Library on [07/11/2026]. See the Terms and Conditions (https://onlinelibrary.wiley.com/terms-and-conditions) on Wiley Online Library for rules of use; OA articles are governed by the applicable Creative Commons License

21699356, 2026, 1, Downloaded from https://agupubs.onlinelibrary.wiley.com/doi/10.1029/2025JB032783, Wiley Online Library on [07/11/2026]. See the Terms and Conditions (https://onlinelibrary.wiley.com/terms-and-conditions) on Wiley Online Library for rules of use; OA articles are governed by the applicable Creative Commons License

The percentage of well resolved magnetic moments in Figure 2a is based on knowing the true magnetic moments of the particles, but for physical samples these are of course not known. Therefore, we computed the SSR that best selects the correctly resolved particles. Remarkably, the SSRs computed for both DSS and SSS are similar with a value of 10^{-2}, and appears to be independent of sample thickness. This static SSR is probably explained by the presence of the millions of modeled undetected grains. Since these particles are unresolved by MMT, they insert extra noise into the magnetic field scan. The resulting noise could be so high that it overshadows other effects. This means that the effect of spatial grain density and number of data points is so low, compared to the noise inserted by these undetected particles, that the thickness of a sample or the amount of data no longer determines whether magnetic moments are well resolved. Figure 2b shows how many particles are resolved when applying this new SSR threshold of 0.01. Overall, less magnetic moments remain when this SSR-proxy is used. This might indicate that well resolved particles are scattered throughout the sample, and the SSR only allows for a partial retrieval of these particles.

In practice, we are mostly interested in the absolute number of particles that are resolved well, as function of surface area of the sample. For both SSS and DSS experiments, the absolute amount of well resolved grains after using the SSR-proxy is relatively stable (Figure 2c). For DSS the amount of resolved particles is slowly decreasing with sample thickness; on average 175 grains are resolved per mm^2 with an occasional dip to 130–140 grains. For SSS this amount decreases from 80 to 90 resolved grains with a 30 micron sample thickness to 50 grains at 100 micron thickness. In all cases DSS outperforms SSS in the number of produced well resolved magnetic moments. Taking the expected difficulties with sample handling of thin samples into account, a sample thickness of 60 μm seems optimal for DSS experiments.

3. Empirical Study

The physical sample is obtained from pillow basalts outcropping in the Philippstein Quarry (Rhenish Massif) near Braunfels, Germany (lat: 50.47°, lon: 8.38°). The sample is of Devonian age and contains euhedral magnetite and some maghemite (de Boer et al., 2023). Although the sample is of Devonian age, we do not concern ourselves with retrieving paleomagnetic information from this sample, but rather use the sample as a test case for DSS. Raw data and processing steps can be retrieved from our repository (Out, de Boer, Walmsley, & de Groot, 2024; Out, de Boer, Kosters, et al., 2024).

3.1. Methods

To make a regular paleomagnetic bulk sample suitable for DSS, a mini-core with a ∼1.6 mm diameter was drilled out of a polished 1 inch diameter ×0.5 cm cylindrical sample. The polished side is glued to a glass plate, after which the other side is polished to reduce the core to a thickness of about 60 μm. Afterward, the glue is removed and a loose sliver with a diameter of 1.6 mm and thickness of ∼60 μm remains; a size that fits both the field of view of NanoCT and QDM (see Figure 3a).

To give the rock sliver a measurable signal, it was pulsed with an isothermal remanent magnetization (IRM) of 8 mT parallel to the sample surface. The sample was placed in the QDM and brought as close as possible to the diamond by the automatic sample stage. During this process, the sample stuck to the diamond, resulting into a top side parallel to the diamond. After scanning one side, the sample was flipped by hand and brought again as close as possible to the diamond by an automatic sample stage. This time the sample did not stick to the diamond, ensuring that the two individual measurements planes are parallel to each other (see Figure 3a). For both cases we applied a microwave frequency from 2,836 to 2,849 MHz and from 2,888 to 2,901 MHz with steps of 260 MHz and measured with a bias field of 0.9 mT using a 8-16-8 protocol, with 20 sweeps per frequency. Each image contains 1200 × 1920 pixels with a pixel size of ∼1.2 μm. The contrast dips in all images were fitted to determine the magnetic field value per pixel.

After the QDM measurements the sample was scanned by the Multiscale X-Ray NanoCT - SkyScan 2211 at the institute of clinical dentistry, University of Oslo, Norway. The scanned sample measures ∼1.7 mm diameter and 0.09 mm thickness with a resolution of ∼460 nm. Figure S1 in Supporting Information S1 shows the pixel values of the raw data. The data were processed with the Dragonfly software package from Object Research Systems (ORS) using a similar approach as described in Out, de Boer, Walmsley, and de Groot (2024) and Out, de Boer, Kosters, et al. (2024). A median filter was applied to the data, after which the images were segmented with a

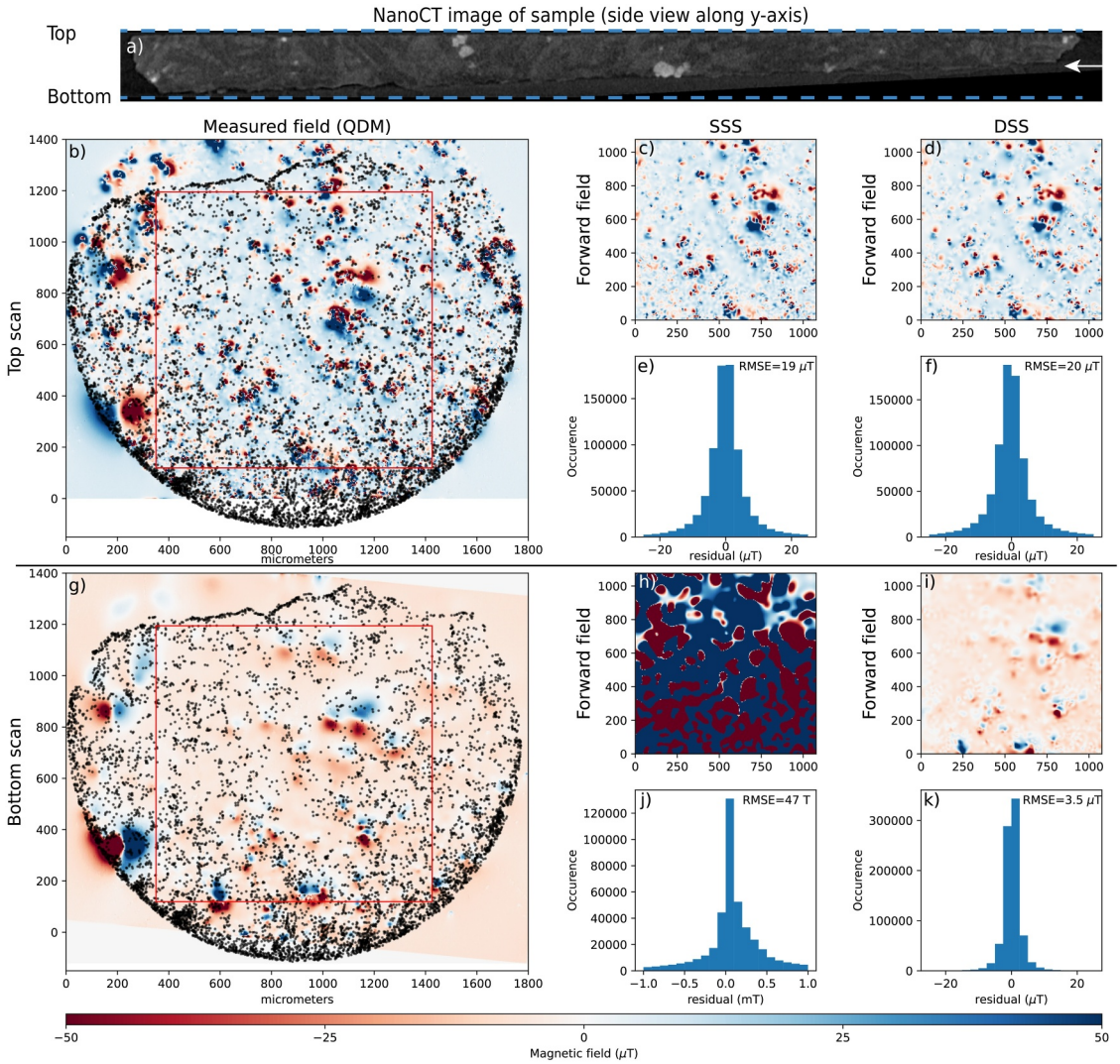


Figure 3. Overview of both measured and modeled QDM scans of the rock sample, accompanied by NanoCT data in the top panel. The smaller panels on the right (c–f and h–k) are calculated forward fields based on iron-oxides (in black) and magnetic field data inside the red outlined regions of panels (b and g). (a) Side-view of NanoCT data of the sample, measuring 1.4 mm length and 40–80 μm thickness. "Top" and "Bottom" refer to QDM measurement planes (see main text). The white arrow indicates that the right side of the sample is thinner than the left side. (b) Measured magnetic field of the top of the sample as shown in panel (a). (c, d) Calculated top magnetic field based on inverting only the top scan (SSS) or both scans (DSS). (e, f) Histogram showing residuals of top magnetic field for SSS and DSS. (g) Measured magnetic field of the bottom of the sample as shown in panel (a). (h, i) Calculated bottom field for SSS and DSS, similar to panels (c and d). (j, k) Histogram showing residuals of bottom field, similar to panels (e and f) (see main text for explanation). Note that the units for panel (j) are in mT.

K-means filter in 4 clusters. The cluster with the highest grain density was used in further processing, since it contains the high-density iron-oxides. Based on the connection of individual voxels, this cluster was separated into 7,463 voxel groups representing individual iron-oxides (Out, de Boer, Walmsley, & de Groot, 2024; Out, de Boer, Kosters, et al., 2024).

After data processing, the reconstructed magnetic sources were fitted in the same coordinate system as the QDM scans using the Dragonfly software package. The top QDM scan defines the coordinate system, so first the NanoCT data was fitted to the LED of this top QDM scan, whereafter the bottom QDM scan was fitted to the NanoCT data. Post-analysis of grain depth, using the algorithm of Souza-Junior et al. (2024), shows that the stand-off distance between the sample and magnetic sensitive layer of the diamond was ∼2 μm for the top scan and ∼4 μm for the bottom scan.

21699356, 2026, 1, Downloaded from https://agupubs.onlinelibrary.wiley.com/doi/10.1029/2025JB032783, Wiley Online Library on [07/11/2026]. See the Terms and Conditions (https://onlinelibrary.wiley.com/terms-and-conditions) on Wiley Online Library for rules of use; OA articles are governed by the applicable Creative Commons License

21699356, 2026, 1, Downloaded from https://agupubs.onlinelibrary.wiley.com/doi/10.1029/2025JB032783, Wiley Online Library on [07/11/2026]. See the Terms and Conditions (https://onlinelibrary.wiley.com/terms-and-conditions) on Wiley Online Library for rules of use; OA articles are governed by the applicable Creative Commons License

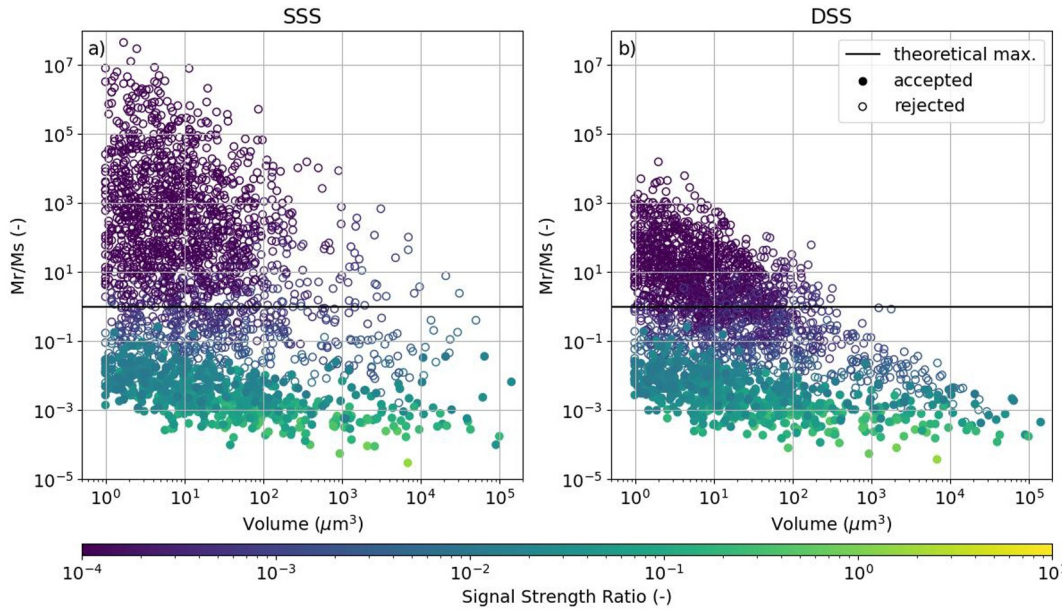


Figure 4. Mr/Ms-ratios of the individual particles sorted by grain volume and colored by SSR retrieved by either SSS or DSS. (a) Mr/Ms-ratio of all particles using SSS. The particles with open circles are filtered out by the SSR-proxy of 10^{-2}. (b) Mr/Ms-ratio of all particles using DSS. The particles with open circles are filtered out by the same SSR-proxy of 10^{-2}.

With all this, everything was set-up to perform the MMT inversion using either SSS or DSS. In both cases we used a 1.1 × 1.1 mm^2 subsection of the full QDM scan and the NanoCT scan with 2,316 particles for the numerical inversion (see Figure S2 in Supporting Information S1 for the grain-size distribution and Figure 3: panel b and g for the measured magnetic fields). This area excludes iron-oxides at the outer rim of the sample since these are probably edge artifacts. For the SSS-case we inverted the top measurement plane for the corresponding magnetic moment with a small modification of the *mmt_multipole_inversion* code of Cortés-Ortuño et al. (2024), and calculated the SSR and Mr/Ms-ratio per grain afterward. The Mr/Ms-ratios were calculated using the volume of each particle as obtained from the NanoCT scan and using the saturation magnetization of magnetite: 480 kA/m. For DSS we used both measurement planes and calculated the same parameters.

3.2. Results

The aim of the experimental part is to show whether DSS delivers more magnetic moments and with higher accuracy than SSS experiments. The improvement in quality becomes evident by the comparison of the calculated (forward) and residual field based on these calculated magnetic moments and the measured field (i.e., the QDM scans) (de Groot et al., 2018). Panels c, d, h, and i in Figure 3 show forward fields of both top and bottom scans using either SSS or DSS, and panels e, f, j, and k show the corresponding histograms of the residual fields with the following root mean square errors (RMSE): 19 μT, 20 μT, 47 T, and 3.5 μT, respectively. For the top QDM scan both SSS and DSS show a forward field similar to the measured field with small residual values. This is expected as SSS and DSS use the top magnetic field as input for allocating magnetic moments. The forward magnetic field shown in panel i is very similar to the input magnetic field, visible in panel g. In contrast to panel i, the forward magnetic field in panel h does not resemble the field plotted in panel g at all. This behavior is caused by the unconstrained magnetic moments of deeper particles resulting into unrealistically high forward fields and hence residuals. The magnetic moments for DSS are well constrained at the bottom and produce small residual fields in panel i. Note that the residuals at the bottom side are lower than for the top side, because the bottom side is measured with a larger distance to the QDM sensor. Therefore, the signals are more smoothed out at the bottom side, ensuring an easier fit and lower residuals.

Figure 4 shows the Mr/Ms-ratios retrieved by either SSS (panel a) and DSS (panel b), colored by SSR (see Cortés-Ortuño et al., 2021; Out et al., 2022). Comparing panel a to panel b indicates that SSS produces higher Mr/Ms-ratios than DSS: DSS produces Mr/Ms-ratios of up to 10^4, while SSS almost doubles this to a

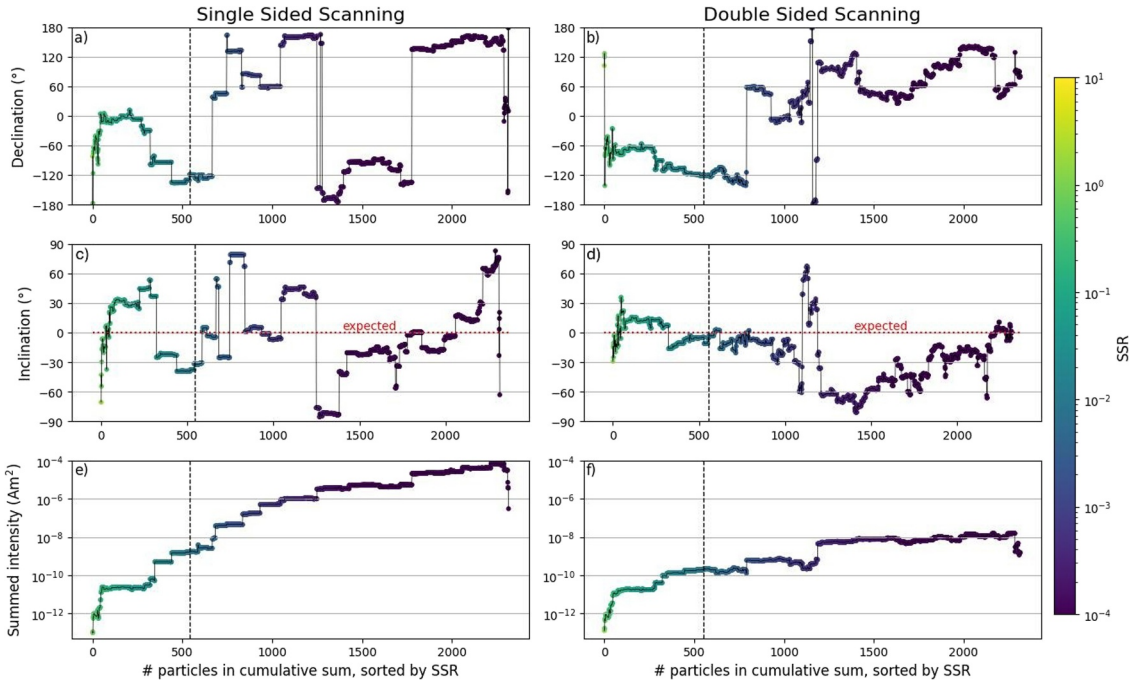


Figure 5. Cumulative plots of declination, inclination, and intensity as function of magnetic carriers sorted by SSR for both SSS (panels a, c, and e) and DSS (panels b, d, and f). The dashed line indicates an SSR value of 10^{-2} (see main text). The dotted line indicates the expected direction for inclination. The Supporting Information S1 contains the same figure sorted by magnetic moment, instead of SSR.

maximum of 10^{8}. SSS is thus outputting more unrealistically high results than DSS, a result which is also shown by the forward magnetic field in Figure 3h. Hence, DSS constrains magnetic moments to more realistic values by considering both the top and bottom scan, providing a closed interval of more realistic solutions for each grain. Both methods return particles with a Mr/Ms-ratio over one, which is physically impossible. After applying a SSR cut-off of 10^{-2} for both SSS and DSS, particles with these unrealistically high Mr/Ms-ratios are completely filtered out for their numerical instability. By ignoring the magnetic moments of these unstable particles, all remaining particles have a realistic Mr/Ms-ratio, well below one; 542 particles for SSS and 554 particles for DSS.

The cumulative signals of all particles for both SSS and DSS are shown in Figure 5. All panels in the figure show that, without constraints, the summed directions and intensities vary intensively when adding particles with the lowest SSR. Evaluating the data up to a SSR threshold of 10^{-2}, indicated by the dashed lines, presents a clear trend: both SSS and DSS show a stable declination of $-120°$ after some initial fluctuations in panels a and b. The trend in inclination, shown by panels c and d, is different for SSS and DSS. While the inclination tends toward zero degrees for DSS, SSS remains around $-30°$. Interestingly, the 8 mT IRM pulse was applied parallel to the sample surface, hence an inclination of zero degrees is expected. The summed intensity, shown in panels e and f, is one order of magnitude lower for DSS than for SSS. Since the cumulative signal for DSS is compiled from grains constrained by a measurement plane below and above, it is to be expected that the resolved grains with DSS have a more conservative magnetic moments than when they would be resolved with a SSS protocol. The stereoplot of SSR-filtered directions for both SSS and DSS, both individual and summed directions, are plotted in Figure S3 in Supporting Information S1. Cumulative magnetic moments sorted by vector size, instead of SSR, for both SSS and DSS are shown in Figure S4 in Supporting Information S1.

4. Discussion

4.1. Theoretical Performance

The numerical part of this study (Figure 2) shows that DSS outperforms SSS for every sample thickness. With SSS, only one measurement plane determines all magnetic moments, resulting into unrealistically high Mr/Ms

21699356, 2026, 1, Downloaded from https://agupubs.onlinelibrary.wiley.com/doi/10.1029/2025JB032783, Wiley Online Library on [07/11/2026]. See the Terms and Conditions (https://onlinelibrary.wiley.com/terms-and-conditions) on Wiley Online Library for rules of use; OA articles are governed by the applicable Creative Commons License

21699356, 2026, 1, Downloaded from https://agupubs.onlinelibrary.wiley.com/doi/10.1029/2025JB032783, Wiley Online Library on [07/11/2026]. See the Terms and Conditions (https://onlinelibrary.wiley.com/terms-and-conditions) on Wiley Online Library for rules of use; OA articles are governed by the applicable Creative Commons License

ratios (Kosters et al., 2023). By measuring both sides of the sample, each carrier is effectively provided with an upper and lower limit, producing significantly more numerically stable magnetic carriers. On the other hand, including data on both sides of the sample into the inversion would require twice as much computer memory. However, by implementing memory-efficient algorithms, we achieved a memory usage similar to the existing algorithm for one sided scans (see modification of the algorithm of Cortés-Ortuño et al., 2024, on Github).

There is a small difference in calculated SSR between this study and the previous SSR study of Out et al. (2022). In that study an SSR dependent on sample thickness is retrieved, between 10^{-3} and $\sim 10^{-2}$. In our study we obtained an SSR of 10^{-2}, independent of sample thickness or whether we use a SSS or DSS protocol. Since we compiled the SSR by adding undetected (ghost) grains (Out, de Boer, Walmsley, & de Groot, 2024; Out, de Boer, Kosters, et al., 2024) to our models, it seems that the effect of other parameters, such as noise and spatial grain density, is of too little influence to effect the instability of the inversion problem further. Adding all these ghost grains is similar to introducing a noise level of $\sim$1 μT to the system. Hence, by improving CT measurement resolution, we can eventually image more of these ghost grains; solving more particles that fulfill our SSR requirement.

4.2. Empirical Performance

DSS resolves more magnetic moments and the corresponding Mr/Ms-ratios are in a more realistic range than for SSS (see Figure 4). However, the amount of particles resolved with DSS for this particular sample, 554 of 2,316 particles (24%), compared to SSS, 542 of 2,316 particles (23%), is less than anticipated by the numerical study. We believe this is caused by the shape of the sample: the top and bottom of the sample are flat and well-polished, but they are not parallel to each other and form a trapezoid (Figure 3a). Because of this shape, the sample has lost many potential numerically stable recorders in the void between the bottom side of the sample and the bottom QDM image surface (see white arrow in Figure 3a). Hence, a parallel top and bottom of a sample is pivotal for acquiring the largest gain with DSS.

Another interesting feature in the experimental data is that both SSS and DSS resolve almost a quarter of the particles, although our numerical study shows that only about 5%–10% of all particles are resolved well in a 80 μm thick sample. We noticed that the grain-size distribution of our studied region is similar to the one used for our numerical study, but that the distribution of particles in depth is not uniform: 30% of the iron-oxide particles reside in the top 10 μm of the sample. A SSR-cutoff of 10^{-2} translates into solving 1 μm grains at a depth of 4 μm. For the same SSR, larger grains can be solved at even greater depths, eventually leading to a quarter of all detected particles fulfilling this SSR cutoff. We think that by using a grain-size distribution that favors small grains (see discussion in Out, de Boer, Walmsley, & de Groot, 2024; Out, de Boer, Kosters, et al., 2024) we overpopulated our numerical models with too many undetected magnetic carriers. This has led to very strict SSR-thresholds thereby compensating for the uneven spatial particle distribution in the empirical sample. This uneven distribution fortuitously led to many particles residing relatively close to the measurement plane, resulting into a large amount of well resolved magnetic moments, which are somewhat aligned to the imposed IRM pulse. Therefore, a strict SSR compensates for differences between the numerical and real sample, and aids in acquiring a higher than expected amount of numerical stable particles for the SSS experiment.

4.3. Sample Geometry and Feasibility

Sample preparation for DSS is more difficult than for SSS. For SSS a thin section that fits the field-of-view of both the NanoCT and the QDM is glued to a glass plate and scanned, but for DSS a sample cannot be glued as it should be freely flippable for scanning both sides without breaking it. According to our numerical study the ideal sample has a diameter not exceeding 1.5 mm and a thickness of 60 micron: the largest thickness that still provides a high amount of stable magnetic moments (see Figure 2c). By polishing the top and bottom side of the sample as parallel as possible, the best data quality and the largest gain of numerically stable moments is ensured. Our experimental sample, on the other hand, has a thickness that varied from $\sim$30 μm on one side to more than 80 μm on the other due to uneven polishing. The thinnest part of the sample broke during preparations for NanoCT measurements inducing a loss of particles (see top of Figures 3b and 3c). Flipping of the sample after measuring one side of the sample, on the other hand, could be successfully achieved with basic lab equipment (i.e., a vacuum tweezer with small nozzle).

21699356, 2026, 1, Downloaded from https://agupubs.onlinelibrary.wiley.com/doi/10.1029/2025JB032783, Wiley Online Library on [07/11/2026]. See the Terms and Conditions (https://onlinelibrary.wiley.com/terms-and-conditions) on Wiley Online Library for rules of use; OA articles are governed by the applicable Creative Commons License

Mapping of QDM data sets onto the CT data can be a major source for intensity errors and angular deviations of the magnetic moments: a horizontal shift of 1 μm of the QDM scan involves angular deviations of more than 10° (see Supporting Information S1). With the Dragonfly software package, however, we could map all data sets with an expected horizontal shift <1 μm within 1 hour. Furthermore, rotation of the QDM scans with respect to the NanoCT images could be minimized to less than 1°. Vertical matching of QDM data to NanoCT data is more difficult to control, because this parameter cannot be checked visually. Furthermore, failing to set this parameter correctly induces very high intensity errors (>100%) in computed magnetic moments. With the algorithm of Souza-Junior et al. (2024), the depth of potential magnetic carriers could be inferred from the QDM scans. By cross-verifying this with NanoCT data, the uncertainty in vertical placement was reduced to less than 1 μm. Through a combination of this algorithm and mapping software, translation and rotation errors were brought to a minimum.

DSS is a major upgrade for MMT as it solves more magnetic moments in thick sections. Our combined numerical and experimental data shows that a sample thickness of about 60 μm is ideal to obtain the largest amount of particles while preventing the sample from breaking. By further optimizing inversion algorithms, larger regions of 1 by 1 mm are inverted at once for DSS: solving an even greater percentage of numerically stable magnetic moments. These extra magnetic moments will help MMT in establishing a statistically significant paleomagnetic direction and intensity through combining the results of sufficient particles (Bellon et al., 2025; Berndt et al., 2016).

5. Conclusions

We showed that it is both numerically and empirically feasible to use magnetic surface scans from both sides of a sample for MMT inversions. DSS is therefore an important addition to the MMT toolbox. From the numerical point of view, DSS doubles the amount of accurately retrieved magnetic moments compared to SSS, with an optimum for a sample thickness of 60 μm. Furthermore, DSS better constrains the magnetic moments of all grains as illustrated by producing realistic Mr/Ms-ratios for more particles. The computational costs for running such an inversion is double the amount for SSS, but by using more efficient algorithms this data overhead is reduced. The experimental part of the study shows that it is possible to obtain magnetic moments with DSS. By preparing a loose sliver of rock of at least 60 μm thick, it can be manually flipped without breaking. Best results are obtained if the top and bottom side are as flat and parallel to each other as possible. The retrieved magnetic moments are overall better constrained and seem to align better with the imposed IRM direction. DSS therefore increases the number of usable particles per sample and constrains magnetic moments to more realistic values, thereby leading to statistically more relevant paleomagnetic information obtained from MMT experiments.

Conflict of Interest

The authors declare no conflicts of interest relevant to this study.

Data Availability Statement

The MicroCT data, QDM data, and codes used for generating the results and figures are available at YODA via https://doi.org/10.24416/UU01-QLA78N with a CC-BY-NC-4.0 license (Out, de Boer, Walmsley, & de Groot, 2024; Out, de Boer, Kosters, et al., 2024). Numerical calculations were executed with support of NumPy (Harris et al., 2020), SciPy (Virtanen et al., 2020), and Matplotlib (Hunter, 2007) Python libraries. The MicroCT analysis for this study was generated using Dragonfly software, Version 2022.1.0.1259 for Windows. Object Research Systems (ORS) Inc, Montreal, Canada, 2022.

Acknowledgments

This project has received funding from the European Research Council (ERC) under the European Union's Horizon 2020 research and innovation program (Grant agreement 851460 to L.V. de Groot). This publication results from work carried out under transnational access action under the support of EXCITE—EC—HORIZON 2020—INFRAIA 2020 Integrating Activities for Starting Communities (Grant agreement 101005611).

References

Bellon, U. D., Williams, W., Muxworthy, A. R., Souza-Junior, G., Nagy, L., Uieda, L., & Trindade, R. I. (2025). Efficiency of thermoremanent magnetization acquisition in vortex-state particle assemblies. *Geophysical Research Letters*, *52*(8), e2025GL114771. https://doi.org/10.1029/2025GL114771

Berndt, T., Muxworthy, A. R., & Fabian, K. (2016). Does size matter? Statistical limits of paleomagnetic field reconstruction from small rock specimens. *Journal of Geophysical Research: Solid Earth*, *121*(1), 15–26. https://doi.org/10.1002/2015JB012441

Cortés-Ortuño, D., Fabian, K., & de Groot, L. V. (2021). Single particle multipole expansions from micromagnetic tomography. *Geochemistry, Geophysics, Geosystems*, *22*(4), 7031. https://doi.org/10.1029/2021GC009663

Cortés-Ortuño, D., Out, F., Kosters, M. E., Fabian, K., & de Groot, L. V. (2024). Micromagnetic tomography: Numerical libraries. *Computers and Geosciences*, *185*, 105555. https://doi.org/10.1016/j.cageo.2024.105555

de Boer, R., van der Boon, A., Königshof, P., & de Groot, L. (2023). Paleomagnetic and micromagnetic measurements of middle Devonian pillow lavas from Germany. In *Egu general assembly conference abstracts* (p. EGU-1885). https://doi.org/10.5194/egusphere-egu23-1885

de Groot, L. V., Fabian, K., Béguin, A., Kosters, M. E., Cortés-Ortuño, D., Fu, R. R., et al. (2021). Micromagnetic tomography for paleomagnetism and rock-magnetism. *Journal of Geophysical Research: Solid Earth*, *126*(10), e2021JB022364. https://doi.org/10.1029/2021JB022364

de Groot, L. V., Fabian, K., Béguin, A., Reith, P., Barnhoorn, A., & Hilgenkamp, H. (2018). Determining individual particle magnetizations in assemblages of micrograins. *Geophysical Research Letters*, *45*(7), 2995–3000. https://doi.org/10.1002/2017GL076634

Dunlop, D. J., & Özdemir, Ö. (1997). *Rock magnetism*. Cambridge University Press. https://doi.org/10.1017/cbo9780511612794

Fabian, K., & De Groot, L. V. (2019). A uniqueness theorem for tomography-assisted potential-field inversion. *Geophysical Journal International*, *216*(2), 760–766. https://doi.org/10.1093/gji/ggy455

Glenn, D. R., Fu, R. R., Kehayias, P., Le Sage, D., Lima, E. A., Weiss, B. P., & Walsworth, R. L. (2017). Micrometer-scale magnetic imaging of geological samples using a quantum diamond microscope. *Geochemistry, Geophysics, Geosystems*, *18*(8), 3254–3267. https://doi.org/10.1002/2017GC006946

Harris, C. R., Millman, K. J., van der Walt, S. J., Gommers, R., Virtanen, P., Cournapeau, D., et al. (2020). Array programming with NumPy [Software]. *Nature*, *585*(7825), 357–362. https://doi.org/10.1038/s41586-020-2649-2

Hunter, J. D. (2007). Matplotlib: A 2D graphics environment [Software]. *Computing in Science and Engineering*, *9*(3), 90–95. https://doi.org/10.1109/MCSE.2007.55

Kosters, M. E., de Boer, R. A., Out, F., Cortés-Ortuño, D. I., & de Groot, L. V. (2023). Unraveling the magnetic signal of individual grains in a Hawaiian lava using micromagnetic tomography. *Geochemistry, Geophysics, Geosystems*, *24*(4), e2022GC010462. https://doi.org/10.1029/2022GC010462

Nagy, L., Williams, W., Muxworthy, A. R., Fabian, K., Almeida, T. P., Conbhui, P. O., & Shcherbakov, V. P. (2017). Stability of equidimensional pseudo-single-domain magnetite over billion-year timescales. *Proceedings of the National Academy of Sciences of the United States of America*, *114*(39), 10356–10360. https://doi.org/10.1073/pnas.1708344114

Out, F., Cortés-Ortuño, D., Fabian, K., van Leeuwen, T., & de Groot, L. V. (2022). A first-order statistical exploration of the mathematical limits of micromagnetic tomography. *Geochemistry, Geophysics, Geosystems*, *23*(4), e2021GC010184. https://doi.org/10.1029/2021GC010184

Out, F., de Boer, R. A., Kosters, M. E., de Groot, B. M., & de Groot, L. V. (2024). Replication data for: Increasing the accuracy and efficiency of micromagnetic tomography by double sided scanning [Dataset]. *YODA*. https://doi.org/10.24416/UU01-QLA78N

Out, F., de Boer, R. A., Walmsley, J., & de Groot, L. V. (2024). The impact of grain-size distributions of iron-oxides on paleomagnetic measurements. *Geochemistry, Geophysics, Geosystems*, *25*(4), e2024GC011512. https://doi.org/10.1029/2024GC011512

Reis, A., Oliveira Jr, V., Yokoyama, E., Bruno, A., & Pereira, J. (2016). Estimating the magnetization distribution within rectangular rock samples. *Geochemistry, Geophysics, Geosystems*, *17*(8), 3350–3374. https://doi.org/10.1002/2016GC006329

Souza-Junior, G. F., Uieda, L., Trindade, R. I., Carmo, J., & Fu, R. (2024). Full vector inversion of magnetic microscopy images using euler deconvolution as prior information. *Geochemistry, Geophysics, Geosystems*, *25*(7), e2023GC011082. https://doi.org/10.1029/2023GC011082

Tauxe, L., & Yamazaki, T. (2015). Paleointensities. In *Treatise on geophysics* (pp. 461–509). Elsevier. https://doi.org/10.1016/B978-0-444-53802-4.00107-X

Virtanen, P., Gommers, R., Oliphant, T. E., Haberland, M., Reddy, T., Cournapeau, D., et al. (2020). SciPy 1.0: Fundamental algorithms for scientific computing in python [Software]. *Nature Methods*, *17*(3), 261–272. https://doi.org/10.1038/s41592-019-0686-2

21699356, 2026, 1, Downloaded from https://agupubs.onlinelibrary.wiley.com/doi/10.1029/2025JB032783, Wiley Online Library on [07/11/2026]. See the Terms and Conditions (https://onlinelibrary.wiley.com/terms-and-conditions) on Wiley Online Library for rules of use; OA articles are governed by the applicable Creative Commons License